Specific Rate Constants $k(E)$ of the Dissociation of the Halobenzene Ions: Analysis by Statistical Unimolecular Rate Theories

William Stevens,[‡] Bálint Sztáray,[§] Nicholas Shuman,[‡] Tomas Baer,*[,‡] and Jürgen Troe[⊥]

Chemistry Department, University of North Carolina, Chapel Hill, North Carolina 27517-3290, Chemistry Department, University of the Pacific, Stockton, California 95211-0110, and Institut für Physikalische Chemie, Universität Göttingen, Tammannstrasse 6, D-37077 Göttingen, Germany

Received: September 6, 2008; Revised Manuscript Received: November 12, 2008

Specific rate constants $k(E)$ of the dissociation of the halobenzene ions $C_6H_5X^+ \rightarrow C_6H_5^+ + X^\bullet$ ($X^\bullet$ = Cl, Br, and I) were measured over a range of 10^3-10^7 s^{-1} by threshold photoelectron−photoion coincidence (TPEPICO) spectroscopy. The experimental data were analyzed by various statistical unimolecular rate theories in order to derive the threshold energies E_0. Although rigid activated complex RRKM theory fits the data in the experimentally measured energy range, it significantly underestimates E_0 for chloro- and bromobenzene. Phase space theory (PST) does not fit the experimentally measured rates. A parametrized version of the variational transition state theory (VTST) as well as a simplified version of the statistical adiabatic channel model (SSACM) incorporating an energy dependent rigidity factor provide excellent fits to the experimental data and predict the correct dissociation energies. Although both approaches have just two adjustable parameters, one of which is E_0, SSACM is effective and particularly simple to apply.

Introduction

Unimolecular dissociation reactions provide an important access to the threshold energies E_0 for bond breaking. The specific rate constants $k(E)$ of these reactions (apart from some fine structure) decrease with decreasing energy E and approach their minimum value as $E \rightarrow E_0$. In order to derive E_0 from $k(E)$, this quantity must be measured experimentally at energies close enough to E_0 that a unique extrapolation is feasible. In addition to the limits imposed by experimental methods for measuring low rate constants, it is not possible to directly measure rate constants less than about 10^2 s^{-1} because of competition from radiative decay.[1,2] In these cases, the difference between the experimental appearance energy of the fragments and the bond energy E_0, the so-called "kinetic shift",[3,4] needs to be determined by fitting the measured part of $k(E)$ to a unimolecular rate theory.[5] Larger molecules have minimum rate constants well below 10^2 s^{-1} and thus require rate constants to be accurate over several orders of magnitude to correctly extrapolate to E_0.

For energy selected reactants, a commonly used model for the specific unimolecular rate constants ($k(E)$) is the Rice−Ramsperger−Kassel−Marcus (RRKM) equation:[5]

$$k(E) = \frac{\sigma N^{\ddagger}(E - E_0)}{h\rho(E)} \quad (1)$$

where $N^{\ddagger}(E - E_0)$ is the sum of states of the transition state, $\rho(E)$ is the reactant density of states, σ is the reaction degeneracy, and h is Planck's constant. In evaluating $N^{\ddagger}(E - E_0)$, it is useful to separate conserved vibrational modes from the transitional modes, which are converted from vibrations into rotational and translational degrees of freedom as the reaction coordinate R goes to infinity. Differences arise in the various rate theories from their treatment of these transitional modes in calculating $N^{\ddagger}(E - E_0)$.

Phase space theory (PST) as advanced by Light, Pechukas, Nikitin, Klots, Chesnavich, and Bowers[6−10] treats $N^{\ddagger}(E - E_0)$ by locating the transition state at either ∞ along the reaction coordinate R, or at the centrifugal barrier. In our treatment we assume the low J limit, for which both models place the transition state at $R = \infty$, at which point the transitional modes have become rotations. Thus, $k(E)$ is determined by the phase space available to the products. This treatment is appropriate for reactions where the interaction potential between the products is isotropic at large separations. At the other extreme is rigid activated complex RRKM theory (RAC-RRKM), in which the transitional modes are treated as vibrations with fixed frequencies. This is appropriate for reactions with real barriers, in which the transition state structure is located at this barrier and does not change with internal energy. However, it is well-known that for reactions with no barrier, the effective transition state, which is related to an entropic minimum, shifts from $R = \infty$ when $E = E_0$ to progressively smaller values as the energy is raised.[5] Several statistical unimolecular rate models have been developed to account for this feature.

In variational transition state theory (VTST), the entropic minimum mentioned above is found by locating the global minimum in the sum of states $N(E - V(R))$ along the reaction coordinate.[11−13] Depending on the implementation of the model, two minima may be found, corresponding to a tight transition state (TTS) at smaller values of R and an orbiting transition state (OTS) at large R.[14] Both minima shift inward as the energy increases, but at some energy an abrupt switch from OTS to TTS may occur. There has been some debate as to whether this transition state switching is physically meaningful in a single-well ionic dissociation, or if only the more gentle transition state shifting occurs, and the two entropic wells are merely an artifact of the approximations used in the interpolation.[15]

An alternative approach to this problem is the statistical adiabatic channel model (SACM) in which the rovibrational

* Corresponding author.
[‡] University of North Carolina.
[§] University of the Pacific.
[⊥] Universität Göttingen.

10.1021/jp807930k CCC: $40.75
Published on Web 12/19/2008

quantum numbers of the reactant are treated as invariant throughout the dissociation by following adiabatic potential curves linking the reactant states and the equivalent product states. Each potential curve has a barrier, the maximum of which moves inward along the reaction coordinate as the energy and angular momentum of the channel increase.[5] A full implementation of either VTST or SACM requires considerable computational effort. Rate constants derived from a full SACM-classical trajectory (SACM-CT) treatment however, have been shown to be reproduced by the much simpler PST with suitable rigidity factors incorporated.[16] Such simplified versions of SACM (SSACM) require no more effort than PST as will be demonstrated below.

It has become clear that in barrierless neutral−neutral dissociations the inward movement of the transition state is significant and RAC-RRKM and PST are insufficient to model the reaction rate.[17] Instead, the extra effort of VTST or SACM is required. The need is less clear, however, in barrierless ionic dissociations. The stronger long-range attraction due to ion-induced dipole interactions causes the transition state to be located at larger values of R. The question then arises whether PST is still insufficient to accurately model the rates.

Troe et al.[16] recently showed that RAC-RRKM fails to predict accurate E_0's in the case of the dissociations of the benzene and butylbenzene cations. However these systems are not ideal for an analysis of kinetic shifts. The former involves a Renner−Teller type avoided curve-crossing between a ground $^2B_1$ and an electronically excited $^2A_1$ state of $C_6H_6^+$.[16,18,19] For the latter system, experimental data[20,21] only exist at higher rates ($k(E) > 10^5$ s^{-1}) which require a large extrapolation to E_0. Additionally, the structure of $C_7H_7^+$ is not known with certainty and the energetics are thus not firmly established. For this reason, we have chosen to investigate other systems which are more suitable for an analysis of kinetic shifts and for the study of energy dependences of specific rate constants $k(E)$. Such systems should fulfill a number of conditions: (i) $k(E)$ should be measurable over a large range; (ii) the thermochemistry of the system should be established sufficiently well by other than kinetic means; (iii) the potential along the dissociating bond should correspond to a simple bond fission, and not show complications such as avoided crossings, small barriers, or reefs.

The halobenzene ion dissociations (2) appear to be suitable systems for the described analysis.

$$C_6H_5X^+ \rightarrow C_6H_5^+ + X^\bullet \quad (X = Cl, Br, \text{and I}) \qquad (2)$$

The dissociation does not involve a curve crossing although both singlet and triplet states of $C_6H_5^+$ may be produced. Experimental values of $k(E)$ can be measured over sufficiently large ranges, in the present work over 4 orders of magnitude, and the thermochemistry of the reactions is relatively well-known. Additionally, the polarizability of the halogens, and therefore the strength of the long-range attraction in the dissociation, increases from Cl to Br to I.

Previous measurements of halobenzene ion dissociation rates have been obtained by numerous workers[22−35] with varying methods, precisions, and ranges of $k(E)$. In this paper, we use threshold photoelectron-photoion coincidence (TPEPICO) to accurately measure the dissociation rate constants over a large range for these three ions and then compare the modeling of these rates with the statistical theories mentioned above in order to determine which methods are appropriate to extrapolate the measured rate constants to their dissociation thresholds.

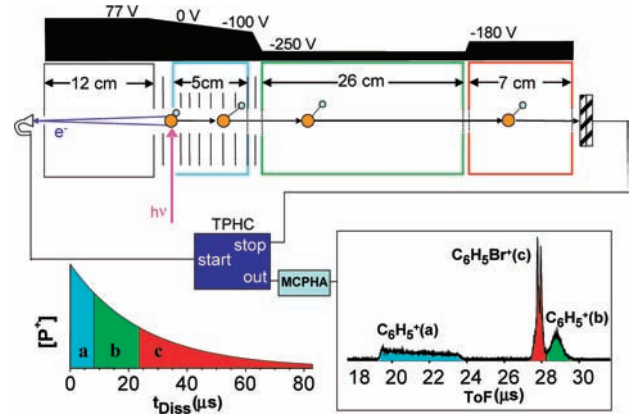

Figure 1. Schematic of the TPEPICO experimental apparatus showing the electron focusing tube and the ion extraction scheme. Ion TOF is a function of both ion mass and lifetime; the color and letter coded exponential decay curve indicates where the ions dissociate and their resulting time-of-flight. The first fragment ion peak is asymmetric because ions are dissociating while accelerating in the 5 cm long acceleration region.

Experimental Technique

All experimental data presented were obtained using the threshold photoelectron−photoion coincidence (TPEPICO) technique that has been described in detail elsewhere,[36−38] and only a brief description is given here. The room temperature sample was introduced through a stainless steel needle into the ion source region of a time-of-flight mass spectrometer. The sample was ionized by vacuum ultraviolet (VUV) light emitted from an H_2 discharge lamp dispersed by a 1 m normal incidence monochromator. The width of the entrance and exit slits was 100 μm, providing a resolution of 1 Å. The wavelength was calibrated using the Lyman-α emission line. Upon ionization, electrons and ions were accelerated in opposite directions in an extraction field of 20 V cm^{-1}. Velocity focusing optics directed electrons having zero velocity perpendicular to the extraction axis onto a 1.3 mm aperture at the end of a 12 cm electron drift region where they were detected by a Burle channeltron detector (see Figure 1). A second channeltron detector collected the background signal of energetic electrons in order to subtract the contamination from energetic electrons flying parallel to the extraction axis. The overall energy resolution was limited by the resolution of the photon monochromator.

Ions were accelerated in the same 20 V cm^{-1} field over 5 cm to 100 eV. A second acceleration region, terminated by grids, increased the ion energy to 250 eV (see Figure 1). A deceleration to 180 eV slowed down fragment ions produced in the long drift region more than parent ions and thus allowed us to separate these fragment ions from their parent ions. The ion time-of-flight (TOF) was measured using a time-to-pulse height converter (TPHC) with the electron signal as the start and the ion signal as the stop. The TPHC signal from each electron−ion coincidence event was recorded by a multichannel pulse height analyzer (MCPHA) thus providing a TOF spectrum. A similar spectrum was collected with the energetic electron detector. Typical acquisition times for TOF distributions varied from 1 to 72 h. To extend the experimental range of the bromobenzene data, spectra were taken using a temperature-controlled inlet[38] set to 256 K and an extraction field of 50 V cm^{-1}. The lowered temperature and steeper gradient improved mass resolution and decreased the time spent in the first acceleration region where we obtain our kinetic information allowing for rates as fast as 10^7 s^{-1} to be observed for bromobenzene. Threshold photo-

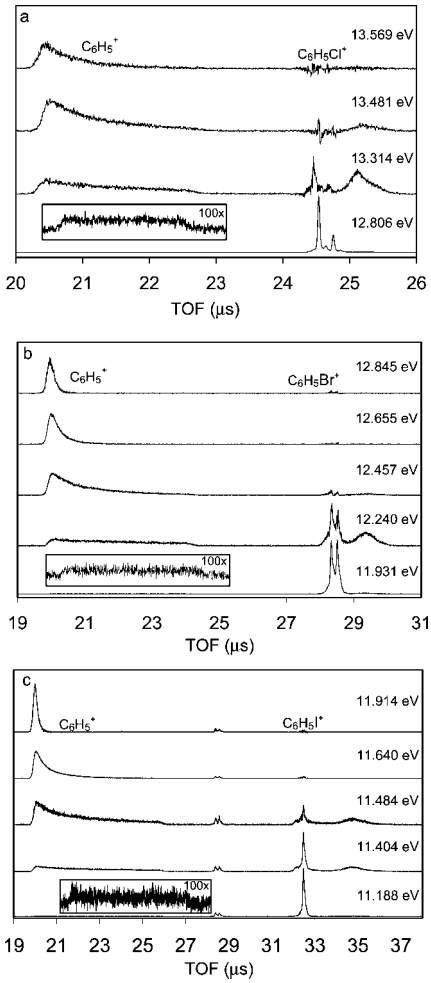

Figure 2. (a−c) Time of flight distributions for the three halobenzene ions at selected photon energies. All spectra have been corrected for energetic electron contamination which accounts for the noise in the region of the parent peak at higher energies. The peak at 28.5 μs in 2c is due to remnant bromobenzene in the sample line, however the bromobenzene ion does not dissociate at these photon energies and does not affect the fragment peak area.

electron spectra of xenon were taken to ensure that the electron energy resolution was not significantly reduced by the increased extraction fields.

Examples of TOF distributions corrected for hot electrons are shown in Figure 2. The isotopic pattern of the parent ion peaks for chlorobenzene is clearly evident at 12.806 eV, where the two chlorine isotopes (35 and 37) as well as the[13] C peaks are fully resolved. At higher energies, the subtraction of the hot electron TOF spectrum eliminates these parent ions (in some cases imperfectly because of the sharp peaks). The broad peak to the right of the parent ion is due to fragment ions that were born in the long drift region.

The breakdown diagrams correspond to the ratio of the peak areas for fragment and parent ions. Examples are shown in Figure 3 for the case of bromobenzene. Two breakdown diagrams are obtained with the ions that fragment between 8.2 and 26.3 μs considered either as fragment ion or as parent ion. The extraction of the rate constants is accomplished by fitting the asymmetric TOF distribution as well as the breakdown diagram.

Rotational constants and vibrational frequencies were calculated using the Gaussian 03 quantum chemical code[39] at B3LYP/6-311++G** for chlorobenzene, bromobenzene, and the phenyl cation and B3LYP/6-311G**[40,41] for iodobenzene. All molecular parameters used to determine the experimental rate constants and employed in the various statistical unimolecular rate constants are reported in the Supporting Information.

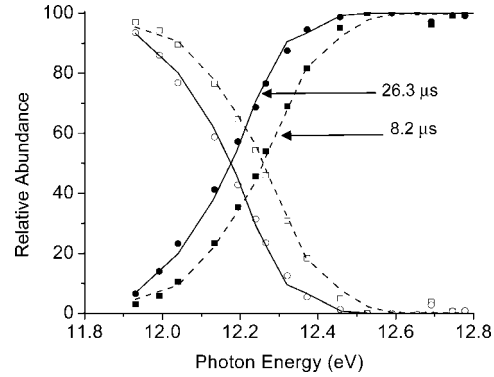

Figure 3. Breakdown curves for bromobenzene. Points are measured relative abundances of parent and daughter ions collected within 8.2 μs (squares) or within 26.3 μs (circles). The respective open points indicate the relative abundance of ions that did not dissociate within that time window. Lines are obtained by fitting the experimental fragment peak shape and relative ion abundances at each photon energy using RAC-RRKM theory at 8.2 μs (---) and 26.3 μs (—)at each photon energy.

TABLE 1: Literature Thermochemical Values Used To Determine Reference E_0s (kJ mol^{-1})

molecule	$\Delta_f H^\circ_{298K}$	$\Delta_f H^\circ_{0K}$	IE (eV)
C_6H_5Cl	52.0 ± 1.3[42]	66.4 ± 1.3	9.0728(6)[43]
C_6H_5Br	105.4 ± 4.1[42]	127.0 ± 4.1	8.9976(6)[43]
C_6H_5I	164.9 ± 5.9[42]	180.7 ± 5.9	8.7580(6)[43]
$Cl^\bullet$	121.302(6)[44]	119.621(6)[44]	
$Br^\bullet$	111.86(6)[44]	117.92(6)[44]	
$I^\bullet$	106.76(4)[44]	107.16(4)[44]	
$C_6H_5^+$		1148.5 ± 3.4[45]	

Thermochemistry of the Dissociations of Halobenzene Ions

Before presenting and analyzing our kinetic data, we briefly inspect the available thermochemical data for the reactions described in equation 2. Assuming that there are no energy barriers for the reverse reactions, the E_0's of the halobenzene dissociations are derived from known heats of formation of the participating species through

$$E_0 = \Delta H^0_{f,0K}(X^\bullet) + \Delta H^0_{f,0K}(C_6H_5^+) - \Delta H^0_{f,0K}(C_6H_5X^+) \quad (3)$$

The heats of formation of the neutral halobenzene molecules C_6H_5X are given in Table 1.[42] They are accurate to ±1.3 kJ mol^{-1} (±13 meV) for chlorobenzene and somewhat less certain for bromo- and iodobenzene. The ionization energies for all three halobenzenes have recently been determined by ZEKE spectroscopy[43] and are accurate within 0.05 kJ mol^{-1}. The values for the halogen atoms are well established.[44] The experimental heat of formation of the phenyl cation was derived[45] from the heat of formation of the phenyl radical[46] and an experimentally determined ionization energy[47] to be 1152.6 ± 4.4 kJ mol^{-1}. However, inspection of the published spectra suggests that the uncertainty in the measurement may have been underestimated. Therefore, we rely here on Ng's recent high-level ab initio calculations giving a value of 1148.5 ± 3.4 kJ mol^{-1}.[45] On the basis of these data the values E_0 = 3.382 ± 0.038, 2.812 ± 0.055, and 2.384 ± 0.070 eV are obtained for the dissociations of chloro-, bromo- and iodo- benzene ions, respectively.

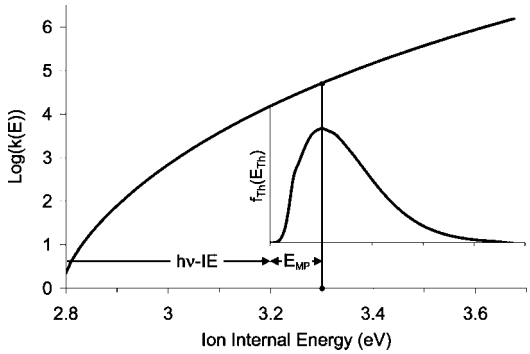

Figure 4. Depiction of the ion thermal energy distribution ($f_{th}(E_{th})$) and corresponding variation in the dissociation rate at a single photon energy. Experimental $k(E)$ for a single ion internal energy are determined from the RRKM $k(E)$ evaluated at the most probable (MP) energy in the ion internal energy distribution ($h\nu - IE + E_{MP}$) as described in the text where $E_{MP} = 56$, 61, and 61 meV for chloro-, bromo-, and iodobenzene, respectively.

Experimental Determination of Specific Rate Constants $k(E)$

The specific rate constants $k(E)$ of the dissociation determine both the abundance of dissociated ions and the shape of the asymmetric fragment peak in the TOF spectrum. However, while our photon resolution is as narrow as 12 meV, our "energy-selected" ions are produced from a room temperature sample of neutrals and therefore correspond to a room temperature thermal energy distribution. Consequently, our experimentally observed dissociation rates are averages over the internal energy distributions of the ions such as illustrated in Figure 4. In order to extract the rate constants as a function of ion internal energy, we convoluted an assumed $k(E)$ function with the thermal energy distribution.

At the lowest experimental energies little information is available from the shape of the fragment peak in the TOF distribution because this distribution is very flat (see Figure 2). At these energies, the rate is mainly determined from the relative peak areas of the parent ions, the asymmetric peak, and the drift peak after the parent ion. However, at higher energies the asymmetric shape of the first peak provides the bulk of the rate information. The largest range of rate constants was accessible for the bromobenzene ion because there are large Franck−Condon factors in the photoelectron spectrum over the full range, which permitted us to obtain rate constants over almost 5 orders of magnitude. In the case of the chlorobenzene ion, the experimental range was limited at high energies by a Franck−Condon gap and the low photon intensity of our light source. At low energies, the range was less than for bromobenzene because of the shorter chlorobenzene ion time-of-flight.

The convolution of the $k(E)$ function with the spectral width of our light source (ca. 12 meV) and the energy distribution of our room temperature sample (ca. 140 meV) was carried out for the TOF distribution and the relative abundances of parent and fragment ions. Denoting a calculated TOF distribution at an energy E by $F(E,t)$ and the thermal internal energy distribution by $f_{th}(E_{th})$, the convoluted TOF distribution $F_{eff}(h\nu,t)$ is given by

$$F_{eff}(h\nu, t) = \int_0^\infty f_{th}(E_{th}) F(h\nu + E_{th}, t)\, dE_{th} \qquad (4)$$

The TOF distribution $F(h\nu + E_{th},t)$, where t is the ion TOF, is directly given by the specific rate constants $k(E)$ at an energy $E = h\nu + E_{th}$, while $F_{eff}(h\nu,t)$ is the observable TOF distribution.

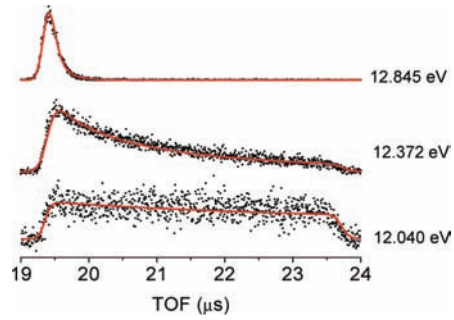

Figure 5. Experimental and modeled fragment peaks for bromobenzene at various photon energies.

TABLE 2: Rate Constants, $\log(k(E))/s^{-1}$, for Chlorobenzene

$h\nu$	E (eV)	expt[a]	RRKM	PST	SSACM	VTST
12.753	3.736	$2.79^{0.10}_{0.09}$	2.80	2.34	2.77	2.75
12.806	3.789	$3.07^{0.10}_{0.09}$	3.07	2.71	3.06	3.09
12.872	3.855	$3.33^{0.09}_{0.05}$	3.38	3.13	3.39	3.43
12.932	3.915	$3.68^{0.32}_{0.11}$	3.55	3.35	3.56	3.59
12.987	3.970	$4.00^{0.30}_{0.20}$	3.87	3.76	3.89	3.91
13.062	4.045	$4.09^{0.46}_{0.01}$	4.17	4.12	4.19	4.20
13.117	4.100	$4.34^{0.40}_{0.07}$	4.37	4.37	4.39	4.39
13.180	4.163	$4.52^{0.29}_{0.08}$	4.58	4.64	4.60	4.60
13.222	4.205	$4.74^{0.18}_{0.13}$	4.72	4.80	4.74	4.74
13.264	4.247	$4.85^{0.10}_{0.07}$	4.86	4.96	4.87	4.87
13.314	4.297	$5.05^{0.07}_{0.08}$	5.01	5.15	5.03	5.02
13.314	4.297	$5.02^{0.15}_{0.06}$				
13.357	4.340	$5.18^{0.04}_{0.09}$	5.14	5.30	5.15	5.14
13.415	4.398	$5.33^{0.09}_{0.05}$	5.30	5.49	5.31	5.30
13.481	4.464	$5.46^{0.10}_{0.04}$	5.48	5.70	5.48	5.47
13.495	4.478	$5.57^{0.19}_{0.11}$	5.52	5.75	5.52	5.51
13.522	4.505	$5.59^{0.24}_{0.08}$	5.59	5.83	5.59	5.58
13.569	4.552	$5.64^{0.15}_{0.06}$	5.71	5.97	5.70	5.69
13.569	4.552	$5.76^{0.35}_{0.08}$				
13.719	4.702	$5.97^{0.14}_{0.07}$	6.07	6.38	6.04	6.03

[a] The superscripts and subscripts represent the upper and lower uncertainties in the experimental values respectively.

The fractional abundances A of the parent and fragment ions observed up to a time τ, are given by

$$A_{parent} = \int_0^\infty f_{th}(E_{th}) \exp[-k(h\nu + E_{th})\tau]\, dE_{th} \qquad (5)$$

and

$$A_{fragment} = 1 - A_{parent} = \int_0^\infty f_{th}(E_{th})(1 - \exp[-k(h\nu + E_{th})\tau])\, dE_{th} \qquad (6)$$

$k(E)$ has to be chosen in such a way that the convoluted TOF distributions $F_{eff}(h\nu,t)$ and the fractional ion abundances from the experiment are reproduced in an internally consistent manner. We achieve this by using an RRKM trial function for $k(E)$ which is locally optimized around the energy of the data point. The procedure provides a unique and correct $k(E)$ at an energy that corresponds to the peak of the thermal energy distribution (Figure 4) and is independent of the trial function. As an example of the analysis of our experimental data, Figure 5 shows a comparison of measured and fitted TOF distributions in the bromobenzene system for a series of excitation energies.

The reported rate constants are those evaluated at the peak of each ion internal energy distribution. They are shown, along with their uncertainties, in Tables 2−4 and in Figures 6 and 7. The given errors were established by observation of the fit to the experimental TOF distributions and breakdown diagrams. The larger errors in the chlorobenzene rates from 3.893 to 4.163

TABLE 3: Rate Constants, log($k(E)$)/s^{-1}, for Bromobenzene

$h\nu$	E (eV)	expt[a]	RRKM	PST	SSACM	VTST
11.931	2.994	$2.64^{0.27}_{0.39}$	2.94	2.11	2.68	2.57
12.04	3.103	$3.51^{0.13}_{0.13}$	3.60	3.10	3.47	3.45
12.134	3.197	$4.03^{0.11}_{0.12}$	4.09	3.77	4.02	4.06
12.194	3.257	$4.35^{0.11}_{0.09}$	4.37	4.14	4.32	4.40
12.240	3.303	$4.58^{0.14}_{0.13}$	4.57	4.40	4.54	4.62
12.266	3.329	$4.74^{0.09}_{0.09}$	4.68	4.54	4.66	4.73
12.321	3.384	$4.97^{0.13}_{0.13}$	4.90	4.82	4.89	4.95
12.372	3.435	$5.20^{0.12}_{0.12}$	5.09	5.05	5.10	5.14
12.457	3.520	$5.49^{0.09}_{0.09}$	5.39	5.42	5.41	5.43
12.527	3.590	$5.69^{0.09}_{0.09}$	5.62	5.70	5.65	5.65
12.590	3.653	$5.92^{0.08}_{0.06}$	5.82	5.93	5.85	5.84
12.655	3.718	$6.13^{0.07}_{0.07}$	6.00	6.15	6.04	6.03
12.681[b]	3.722	$6.02^{0.10}_{0.05}$	6.01	6.54	6.37	6.35
12.778	3.841	$6.43^{0.10}_{0.07}$	6.34	6.71	6.52	6.49
12.845	3.908	$6.56^{0.16}_{0.13}$	6.49	6.16	6.05	6.04
12.919[b]	3.960	$6.62^{0.10}_{0.10}$	6.63	6.88	6.66	6.63
12.976[b]	4.017	$6.72^{0.09}_{0.07}$	6.76	7.03	6.79	6.76
13.022[b]	4.063	$6.81^{0.07}_{0.08}$	6.86	7.14	6.89	6.86
13.069[b]	4.110	$6.89^{0.09}_{0.05}$	6.97	7.27	7.00	6.96
13.145[b]	4.186	$6.93^{0.07}_{0.06}$	7.12	7.44	7.15	7.11

[a] The superscripts and subscripts represent the upper and lower uncertainties in the experimental values respectively. [b] Measurements taken at 40 V/cm and 256 K.

TABLE 4: Rate Constants, log($k(E)$)/s^{-1}, for Iodobenzene

$h\nu$	E (eV)	expt[a]	RRKM	PST	SSACM	VTST
11.188	2.491	$2.64^{0.34}_{0.25}$	2.73	2.45	2.75	2.63
11.234	2.537	$3.16^{0.09}_{0.22}$	3.21	3.03	3.22	3.13
11.275	2.578	$3.61^{0.19}_{0.16}$	3.59	3.48	3.59	3.54
11.326	2.629	$4.00^{0.17}_{0.07}$	4.00	3.94	4.01	3.98
11.378	2.681	$4.42^{0.04}_{0.14}$	4.37	4.34	4.39	4.37
11.404	2.707	$4.53^{0.07}_{0.07}$	4.53	4.53	4.56	4.55
11.431	2.734	$4.72^{0.07}_{0.10}$	4.70	4.71	4.73	4.73
11.457	2.760	$4.86^{0.07}_{0.13}$	4.86	4.87	4.88	4.89
11.484	2.787	$5.03^{0.07}_{0.13}$	5.01	5.04	5.03	5.05
11.537	2.840	$5.27^{0.06}_{0.10}$	5.29	5.34	5.31	5.34
11.586	2.889	$5.56^{0.03}_{0.10}$	5.53	5.59	5.55	5.57
11.640	2.943	$5.74^{0.09}_{0.03}$	5.77	5.85	5.79	5.78
11.706	3.009	$6.04^{0.09}_{0.09}$	6.05	6.14	6.06	6.02
11.756	3.059	$6.19^{0.11}_{0.08}$	6.25	6.35	6.25	6.19
11.914	3.217	$6.73^{0.27}_{0.12}$	6.80	6.92	6.79	6.67

[a] The superscripts and subscripts represent the upper and lower uncertainties in the experimental values respectively.

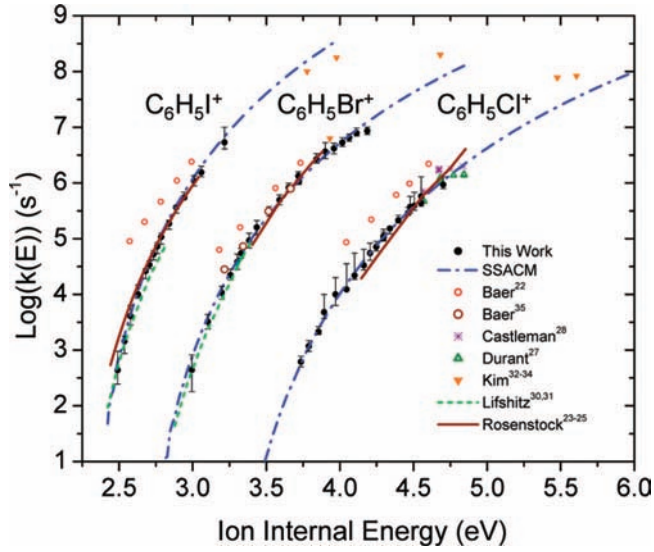

Figure 6. Comparison of current experimental data with previously reported data. SSACM curves are calculated using the parameters that best describe the data presented in this paper. The names in the legend are those of the corresponding authors who reported the data and superscripts refer to their citations. For a detailed discussion of previous data see text. All $k(E)$ data have been adjusted to reflect the most current ionization energies reported in Table 1.

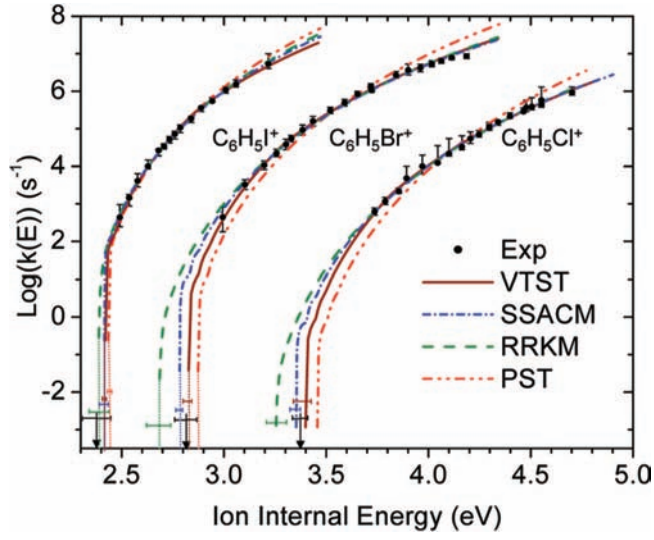

Figure 7. Comparison of rate curves predicted by several models (see text) of statistical unimolecular dissociation fit to experimentally determined rate points. Literature dissociation thresholds (E_0) are indicated by black arrows. Dotted vertical lines for iodo and bromobenzene are to guide the eye from lowest $k(E_0)$ point to the horizontal axis. The determination of errors bars in rate points and E_0 is described in the text.

eV and in the bromobenzene rates from 3.136 to 3.323 eV reflect a discrepancy between the rate constants derived from the fragment peak shapes and those derived from the relative areas of the fragment and parent peaks. Before comparing the measured rate constants to the calculated dissociation rate constants, it is important to establish whether at low energies the ions could be stabilized by IR emission. Such an emission would effectively stabilize the parent ions and yield a daughter to parent ratio that is too low. The IR emission rates, calculated using the method described by Dunbar[48] with frequencies and IR emission intensities calculated using Gaussian 03,[39] were similar for all three systems and ranged from about 100 photons$\cdot s^{-1}$ at 2.4 eV internal energy to 450 photons$\cdot s^{-1}$ at 5 eV. Although IR emission is competitive with dissociation at the lowest experimental energies, the effect on the extracted rate constants is much smaller than the reported error bars.

The measured rate constants range from 3×10^2 s^{-1} to 10^7 s^{-1}, a range of over 4 orders of magnitude. A number of groups have previously determined halobenzene ion dissociation $k(E)$ rates using a variety of techniques and covering selected regions of the $k(E)$ curve (Figure 6).[22−35] Baer et al.[22] reported rate constants for all three molecular ions that were obtained by fitting the TPEPICO TOF distributions for the room temperature sample with a single exponential decay. These points have rates that are too high. In a subsequent paper[35] the rates for the bromobenzene ion were analyzed in terms of a distribution of single exponential decays over the thermal energy distribution, resulting in rate constants that are in agreement with the current measurements. In a series of three papers, Rosenstock et al.[23−25] measured k(E) for the three ions by fitting an RRKM curve to breakdown diagrams obtained by TPEPICO at two ion extraction times. These rate constants, which extend between 2−3 orders of magnitude, agree well with the current data. In 1984, Durant et al.[27] used a supersonically cooled sample of chlorobenzene

to investigate the ion dissociation rates in the vicinity of $k(E)\sim10^6$ s^{-1} by multiphoton ionization time-of-flight mass spectrometry. A few years later, Castleman et al.[28] used a similar technique to study the chlorobenzene ion dissociation over a similarly limited range of rate constants by varying the reflector voltage in a reflectron-time-of-flight apparatus. None of these investigations reported rate measurements below about 5×10^4 s^{-1}, which means that they were not very useful for extrapolating the rate measurements to the dissociation threshold. However, Lifshitz et al.[30,31] performed a series of measurements using an ion trap, which could store the ions for up to milliseconds and could thus explore the critical low rate constant region for the case of bromo- and iodobenzene. Although the ions were not energy selected, the ion internal energy distribution obtained by single photon ionization was modeled and the ratios of the fragment and parent ions as a function of both photon energy and ion extraction time where reproduced using RRKM rate curves. This provided rates in the 10^2-10^5 s^{-1} range, which as shown in Figure 6, agree quite nicely with our reported rate constants. Finally, Kim et al.[32−34] measured the $k(E)$s of iodo-, chloro-, and bromobenzene by mass-analyzed ion kinetic energy spectrometry (MIKES) in which ions prepared by charge transfer were photodissociated as they were traveling at high velocity toward an electric sector of a double focusing mass spectrometer. With the exception of one measurement for bromobenzene at a rate of 10^7 s^{-1}, which agrees with our rate constants, this yielded rates in the region of about $k(E) \sim 10^8$ s^{-1}, which for bromo- and chlorobenzene are clearly higher than the extrapolated rate constants using the SSACM model. Because we did not measure rate constants up to 10^8 s^{-1}, we cannot be certain that the Kim rate constants are in error. However, it is worth mentioning that ion energy selection by charge transfer depends upon the assumption that the ionizing ion (Xe^+ for chlorobenzene and CS_2^+ for bromo- and iodobenzene) be in the ground-state and that the charge transfer process is strictly resonant so that no energy is lost to translation.

Modeling the Rate Constants $k(E)$ by Statistical Unimolecular Rate Theories

The lowest energy rate points measured are between 0.1 and 0.4 eV above E_0. In order to extrapolate the rate curves down to threshold we model the dissociations using several forms of statistical unimolecular rate theory: RAC-RRKM, PST, SSACM, and VTST (Figure 7). These approaches all use the same density of states in the denominator of eq 1, but differ in the manner in which the sum of state, $N^{\ddagger}$, is calculated. We have made the assumption that the various excited electronic states initially populated in the ionization process rapidly interconvert to the ground ionic state, thereby converting their electronic energy into vibrational energy of the ground state. However, ions are free to interconvert electronic and vibrational energy among the several electronic states that lie below the dissociation limit. We tested the contribution of the excited electronic state to the total density of states and found that even for the case of chlorobenzene, in which the upper spin orbit state lies only 100 meV above the ground state, the contribution is less than 10%. Such small differences are negligible and are generally compensated by assumed transition state frequencies.

Rigid Activated Complex RRKM Theory (RAC-RRKM): In RAC-RRKM[5] theory, $N^{\ddagger}$ is determined by the vibrational frequencies of the transition state, which we express by means of the calculated equilibrium frequencies of the halobenzene ion. The frequency corresponding to the C−X stretch is assumed to correspond to the reaction coordinate and is omitted from the transition state. The 27 vibrational modes of the phenyl ring are assumed to be conserved along the reaction coordinate, and the frequencies of the remaining 2 modes, corresponding to C−X bends, are scaled by a common factor. Two parameters, this frequency scaling factor and E_0, are optimized to find a best-fit to the experimental data.

The molecular parameters and the parameters used in the fitting are summarized in the Supporting Information. One should note that there are ambiguities even in this simple RAC-RRKM approach because, apart from the uncertainties in the frequency set, the contribution of anharmonicity can only be guessed. An energy-independent anharmonicity factor $F_{anh} = 1.4$ was adopted by Klippenstein et al.[18] for the case of H loss from benzene ions. However, this ignores the fact that F_{anh} is energy dependent.[5] Here we take $F_{anh} = 1.0$ and include the effects of anharmonicity in the fitted transition state frequency scaling parameter. The experimental $k(E)$ curves can be fit well by this RAC-RRKM modeling, however, the resulting bond energies underestimate the chloro- and bromobenzene thermochemical values from section 3 by 0.13 eV, well outside the thermochemical uncertainties. Of the fitted values, only the iodobenzene value is within the uncertainty of the literature value. Tables 2−4 compare the RAC-RRKM $k(E)$ results with the experimental data.

The good agreement between the RAC-RRKM derived E_0 and the thermochemical value for the iodobenzene ion dissociation is the result of the low E_0 which causes the minimum rate $k(E_0)$ to be larger and therefore the kinetic shift to be smaller. For bromobenzene, in addition to inaccurately predicting the E_0, the described RAC-RRKM modeling was unable to provide good agreement simultaneously at the upper and lower extremes of the data set. The results for chlorobenzene demonstrate most clearly the shortcomings of the RAC-RRKM method. The experimental chlorobenzene data set extends over the smallest experimental range (3 orders of magnitude), and requires the largest extrapolation to E_0. These two factors allow for a "worst case scenario" where the modeling in Figure 7 reproduces the chlorobenzene data deceivingly well over the entire data set but nevertheless predicts a dissociation energy that is too low by 0.13 eV.

Phase Space Theory (PST). The underestimation of E_0 by RAC-RRKM theory agrees with the observations made by Troe et al.,[16] namely that RAC-RRKM fails because it treats the activated complex with a set of vibrational oscillators, resulting in a $k(E)$ function with too weak an energy dependence. One then might think that PST is more appropriate for ionic dissociations, because it considers the activated complex at $R = \infty$, where the transitional modes are rotations and the energy dependence of $k(E)$ is much stronger. In this case, the activated complex frequencies are those of the phenyl product ion. The density of states of these "conserved oscillators" is then convoluted with the relevant number of states $N_{orb}(E)$ of the orbital motion of the fragments. We simplify any rotational effects by using only $k(E,J = 0)$ for which $N_{orb}(E) \approx (E - E_0)/B_{eff}$ and $B_{eff} = (ABC)^{1/3}$,[49] thereby treating the phenyl ion as a spherical top. The J-dependence of $k(E,J)$ in this case is known to be small and can practically be neglected if E is identified with the vibrational energy.[16] However, it must be accounted for through $E_0(J)$ when thermal rate constants for dissociation or the reverse combination are calculated. We again neglect anharmonicity ($F_{anh} = 1.0$) and note that there are considerable uncertainties in the frequencies of the phenyl cation (see Supporting Information). The two frequency sets employed by Klippenstein[19] lead to differences in $k(E)$ by about a factor of

TABLE 5: Dissociation Energies E_0 (eV) for $C_6H_5X^+ \rightarrow C_6H_5^+ + X$ (See Text)

	reference E_0	RRKM	PST[b]	SSACM[a]	VTST[a]
$C_6H_5Cl^+$	3.382 ± 0.038	3.253 ± 0.05	3.457	$3.355^{0.030}_{0.040}$	$3.401^{0.017}_{0.062}$
$C_6H_5Br^+$	2.812 ± 0.055	2.684 ± 0.06	2.874	$2.783^{0.026}_{0.029}$	$2.829^{0.012}_{0.030}$
$C_6H_5I^+$	2.384 ± 0.070	2.387 ± 0.05	2.435 ± 0.01	$2.415^{0.020}_{0.027}$	$2.420^{0.010}_{0.011}$

[a] The superscripts and subscripts represent the upper and lower uncertainties in the experimental values respectively. [b] Due to poor fits to the experimental data, uncertainties are not reported for chlorobenzene and bromobenzene.

2. Regardless of this ambiguity, using the frequencies determined here, the PST $k(E)$ (Figure 7) provides a good fit to the iodobenzene ion experimental $k(E)$, but not to the chloro- or bromobenzene ion data. The only parameter, E_0, is varied in order to fit the PST rates at an energy near the middle of the experimental data set. This leads to values of E_0 that are larger than the thermochemical values. Apart from the uncertainties in the frequency set and the anharmonicity factor, the PST model of $k(E,J = 0)$ is a single-parameter fitting approach which provides upper limits of E_0. We note that the PST rate curve anchored at the literature value of E_0 provides a good fit to the experimental rates below 10^5 s^{-1} for the bromobenzene ion and below 10^4 s^{-1} for the chlorobenzene ion, but significantly overestimates the higher energy rates.

The overestimation of $k(E)$ by PST, if the true E_0 is chosen, is a general phenomenon which, within the framework of the SACM, is attributed to the anisotropy of the potential energy surface and is characterized by a "rigidity factor" f_{rigid} being smaller than unity. One might try to represent this effect by an increased value of B_{eff} in $N_{orb}(E)$, which corresponds to an energy-independent value of f_{rigid} such as was proposed in the simplest version of a "simplified SACM" (SSACM).[50] Adopting this approach here and fitting the scaling factor of B_{eff} in the middle of the experiments still overestimates the true E_0. Although this approach accounts for some rigidity of the activated complexes, it does not do this in an adequate manner when large energy ranges are considered. A more realistic procedure requires energy-dependent rigidity factors such as discussed in the following section. Alternatively variational transition state theory (VTST) may also be used and is described after the SSACM discussion. In these models, there will be a gentle "shifting" or a more abrupt "switching" of the effective transition states from larger fragment distances at lower energies to smaller distances at higher energies. As a result, $k(E)$ with increasing energy falls increasingly below the PST values.

Simplified SACM(SSACM) for Ion Dissociation. Rigidity factors $f_{rigid}(E)$ reflect the anisotropy of the potential and, in addition, the subtle interplay between the anisotropic and attractive properties of the potential; i.e., they are specific for particular types of potential energy surfaces of the dissociation process.[51] In some cases, like ion fragmentations dominated by long-range ion-permanent dipole forces,[52] f_{rigid} is energy independent, but strongly depends on angular momentum J. In other cases like ion fragmentations governed by a superposition of polarizability and permanent dipole contributions, E- and J-dependences of $f_{rigid}(E,J)$ arise.[51] Energy-dependent rigidity factors $f_{rigid}(E)$ are also typical for ion fragmentations which at short-range are dominated by valence forces and at long-range by comparably weak ion-induced dipole forces. A detailed SACM/CT treatment was applied[16] to systems of this type. The results could approximately be described by a functional form of $k(E)$ in which $N_{orb}(E)$ is used from PST and is multiplied by an energy-dependent rigidity factor given approximately by

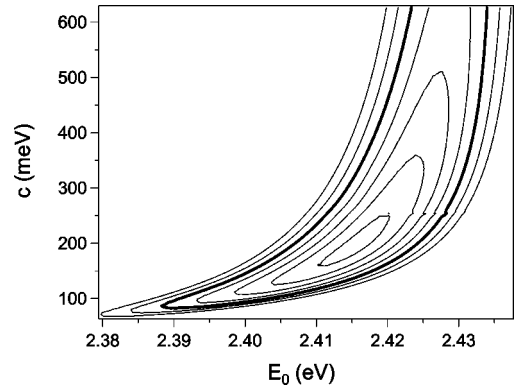

Figure 8. The two-parameter c versus E_0 plot used to determine the best fit SSACM $k(E)$ curve for the experimental rate constants for iodobenzene. The bold contour represents the maximum error that defines an acceptable fit.

$$f_{rigid}(E) = \exp[-(E - E_0)/c] \quad (7)$$

This version of a SSACM was shown to mimic the transition state shifting or switching and found to reproduce quite well the results of the full SACM/CT calculations on modeled potential energy surfaces for the fragmentations of benzene and *n*-butylbenzene cations.

Similar to RAC-RRKM theory, this version of SSACM contains two adjustable parameters, E_0 and c. In order to determine the best-fit E_0 and the corresponding uncertainty, we calculate a least-linear squares error between the calculated and experimentally determined rate curves for all reasonable combinations of E_0 and c. The results are recorded in Figures 6 and 7 and Tables 2−5. Our best fits correspond to values of $E_0 = 3.355^{0.030}_{0.040}$, $2.783^{0.026}_{0.029}$, and $2.415^{0.020}_{0.027}$ eV, where the superscripts and subscripts respectively correspond to the upper and lower uncertainties, and $c = 71$, 77, and 194 meV for chloro-, bromo-, and iodobenzene, respectively. The meaning of the c parameter will be discussed later.

We obtain the error limits for the onset energies by calculating a least-squares error between the calculated and experimentally determined rate curves for all reasonable combinations of E_0 and the fit parameter c (Figure 8). The reported E_0 corresponds to the best fit value, while the uncertainties correspond to the limits of a goodness-of-fit contour (Figure 8, bold contour) beyond which the agreement of the rate curves is determined to be poor. The relationship between E_0, the fit parameter c and the resulting error bars are plotted in figure 9 for the three halobenzenes. Figures 8 and 9 show the origins of the sometimes asymmetric error bars. The nearly vertical line in the case of iodobenzene indicates that, within the experimental window, $k(E)$ is independent of c and is therefore described well by PST.

Microcanonical Variational Transition State Theory (VTST): Microcanonical VTST locates the transition state at the minimum in the $N(E,R)$ along the reaction coordinate R, which moves to shorter bond distances with increasing E. Obtaining $N(E,R)$ requires knowledge of both the interaction potential and transitional modes along R.

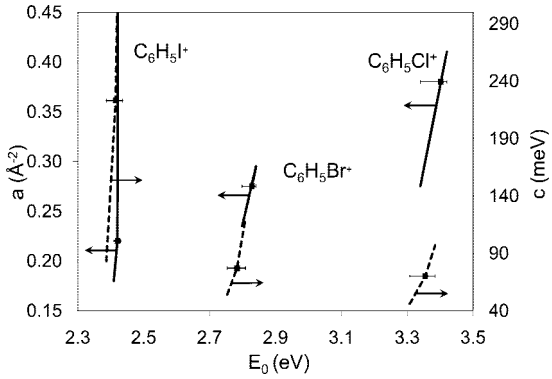

Figure 9. Combinations of E_0 and fitting parameter (see text) determined by VTST (solid, left axis) and SSACM (dashed, right axis) that yield an acceptable fit to the experimentally determined rate curves. Points are the best fit parameters and the limits of the whiskers are the derived uncertainties in E_0.

Below is a simplified approach to obtaining *N(E,R)* proposed by Chesnavich et al.[14] For this version of VTST, the potential is approximated by

$$V_{CX}(R) \approx \frac{D_e}{c_1 - 6}\{2(3 - c_2)\exp[c_1(1 - X)] - (4c_2 - c_1c_2 + c_1)X^{-6} - (c_1 - 6)c_2X^{-4}\} \quad (8)$$

where X is the reduced length, $X = R/R_e$, of the dissociating bond, D_e is the dissociation energy corrected for the zero point energy, $c_2 = \alpha q^2/2R_e^4D_e$ with the polarizability α of the halogen atoms, q is the ionic charge, and c_1 is determined by the force constant of the C−X stretch. These quantities are calculated and given in the Supporting Information. We note that the corresponding quantum-chemical potentials for chloro- and bromobenzene[19] are more repulsive than this empirical potential in the important region between 3 and 5 Å. We will return to this point below and highlight the relative unimportance of an accurate reaction coordinate potential in the VTST scheme.

The contribution of the transitional modes, which for the halobenzene dissociation are the two C−X bending modes, to $N_{tot}(E,R)$ was determined using a hindered rotor potential of the form

$$V(\theta) = \frac{V_0(r)}{2}(1 - \cos 2\theta) \quad (9)$$

The rotational barrier V_0 is a function of the bond length R of the form

$$V_0(r) = V_e \exp[-a(R - R_e)^3] \quad (10)$$

where a is a fit parameter that determines how quickly the rotational barrier decays as a function of bond length, and therefore the rate of "loosening" of the transitional modes. The equilibrium barrier heights V_e were calculated from the geometrical means of the equilibrium C−X bending frequencies and were derived to be 7.85, 5.92, and 4.85 eV for chloro-, bromo-, and iodobenzene, respectively. The exponent in (10) differs from the Gaussian form proposed by Chesnavich and used in previous studies.[14,29] In modeling the $k(E)$ data with VTST, we found that raising the $(R - R_e)$ function to the third power provided a better fit over the full range of the data, and more importantly, provided a much tighter fit (with uncertainties of ±3 kJ mol^{-1} as opposed to ±7 kJ mol^{-1}). Energy levels for the transitional modes, E_i, were calculated using a harmonic oscillator $E_i < V_0(R)$ and a Pitzer rotor model for $E_i > 0.75V_0(R)$. $N_{tot}(E,R)$ was determined by convoluting the phenyl cation density of states with the contribution from the transitional modes. In all three reactions we found two minima of $N(E,R)$ along the reaction coordinate R, an outer TS at very large bond distances ($r > 15$ Å), where $N(E,R)$ is independent of the parameter a, and a tight TS in the range $3 < r < 5$ Å where $N(E,r)$ strongly depends on a. At small E, the outer minimum is the global minimum; as E increases, the inner minimum increases at a slower rate and eventually determines the rate.

We obtained an optimum fit to the experimental $k(E)$ with the parameters $E_0 = 3.401^{0.017}_{0.062}$, $2.829^{0.012}_{0.030}$, and $2.420^{0.010}_{0.011}$ eV and $a = 0.38$, 0.28, and 0.22 Å^{-2} for chloro-, bromo-, and iodobenzene, respectively. The VTST results are plotted with experimental $k(E)$ for comparison in Figure 7 and listed in Tables 2−5. The uncertainties in E_0 were determined in the same way as for the present SSACM, and are included in Figure 9.

Table 5 compares the E_0 values obtained by the different approaches. In the cases of chloro- and bromobenzene, RAC-RRKM extrapolates to too low a barrier, PST to too high a barrier, while both VTST and SSACM extrapolate to barriers within mutual uncertainty of the literature values. All four methods correctly extrapolate to E_0's within the uncertainty of the literature value of the iodobenzene ion dissociation.

Discussion

Neither the RAC-RRKM nor PST approaches correctly extrapolate to the reaction barriers for the chloro- and bromobenzene ion dissociations explored here or the benzene and *n*-butylbenzene ions previously studied.[16] Of particular concern is the fact that the RAC-RRKM theory is perfectly capable of fitting data over a broad range of rates from 10^3 to 10^7 s^{-1} and provides no clues about its inability to extrapolate to the onset. Thus, if the predicted kinetic shift is greater than about 0.2 eV, it is best not to apply RAC-RRKM for extrapolation. In contrast, both the VTST and SSACM approaches correctly determine E_0 for not only the iodobenzene but also the chloro- and bromobenzene ion dissociations.

The VTST and SSACM models produce nearly identical rate curves over the experimental range, along with similar E_0s and uncertainties. The VTST calculation requires an assumption about the potential energy function along the reaction coordinate, whereas the SSACM requires only the product vibrational and rotational frequencies. Additionally, the SSACM rate curve can be calculated using 2 orders of magnitude less computational effort than our VTST curve. In fact, it requires no more effort than the RAC-RRKM method.

What physical insight does the functional form of eq 7 and the values of the parameter c provide? The energy-dependence of $f_{rigid}(E)$ signals a potential with changing anisotropy character, being strongly anisotropic at short-range where valence forces dominate and being nearly isotropic at long-range where ion-induced dipole forces are relevant. The values of the parameters c, being 71, 77, and 194 meV for chloro, bromo, and iodobenzene, respectively, are of the same order as observed in benzene and *n*-butylbenzene cation dissociations.[16] In an intricate manner they reflect the transition from the anisotropic to the isotropic region of the potential. The larger value of c for iodobenzene indicates that the relative contribution of the isotropic long-range part of the potential in comparison to the anisotropic short-range part is larger than for chloro- and bromobenzene, due to the smaller value of E_0. However, a more quantitative connection to details of the potential would require the full SACM/CT treatment on the complete potential energy surface. This is beyond the scope of our present work.

It might appear that our version of VTST provides more dynamical information than SSACM because we identify the entropy bottleneck directly by minimizing the sum of states. However, we found that our empirical potential, fitted to some of the molecular properties of the ion, does not correspond well with a DFT calculated interaction potential. Furthermore, when we replace the empirical potential with a DFT calculated curve, or even a simple Morse potential, the *a* parameter changes, but the overall fit of the rates to the data and its ability to extrapolate to the onset is not affected. This means that our approach is simply a procedure that reproduces the data using an adjustable parameter. The empirical VTST approach also does not lend much insight into the question of transition state switching versus a smooth transition from PST at low energy to RRKM at high energy. For instance, we observe an abrupt transition-state switch at 10^4 s^{-1} for chlorobenzene and at 10^5 s^{-1} for the bromobenzene ion dissociations. However, the energy at which the switch occurs is highly dependent on the specifics of the model. The data can be well fit and the switch occur inside the experimental range, outside that range, or not at all depending on the treatment of the transitional modes (i.e., the value of the *a* parameter and the form of equation 10). Further insight about the issue of transition state switching can be found in discussions by Klippenstein[19] and Hase.[15] On the basis of our results, we conclude that the *a* parameter is effectively a catch-all fitting parameter, much like the *c* parameter in the SSACM or the frequency scaling factor in RAC-RRKM. On the one hand this robustness lends confidence in the results of the calculation in that incorrect assumptions about the potential energy surface do not bias the results, but on the other hand, it means that *a* does not have a precise meaning.

Because both VTST and the SSACM provide similar results and similarly limited physical insight into the dissociations, the considerably simpler SSACM is the preferred approach. Although VTST and SSACM both predict E_0s that are within the experimental error, the error limits are smaller than those of the experiment, and the two theories systematically differ in that the VTST approach yields slightly lower E_0s than does the SSACM, and their predictions in the case of chloro- and bromobenzene are just beyond the error of each method. Both methods predict a considerably higher E_0 for iodobenzene, which means that the experimental values for the heat of formation of iodobenzene should probably be lowered by 3 kJ mol^{-1}. If the precision of the thermochemistry of the halobenzene ion dissociations could be improved, it could decide whether VTST or SSACM approaches are more accurate. Finally, it is worth noting that the version of SSACM used is essentially a first order correction to the PST and is thus most accurate at low energies. As the energy is increased, the employed rigidity factor decreases faster than the PST $k(E)$ increases and the calculated reaction rates become too slow, even decreasing at higher energies, which is clearly not in accord with experiment. This can be corrected for by adding a small energy independent term to eq 7. The VTST rate curves do not suffer from this same problem, however their accuracy at higher energies are untested.

Whether the VTST or SSACM method is used, the accuracy of the derived E_0 values is highly dependent on the quality and range of the experimentally determined rate curves. The uncertainties in E_0 scale roughly linearly with the uncertainties in the experimental rates and are very sensitive to the range of the experimental data. For chlorobenzene, excluding rates below 10^4 s^{-1} from our analysis doubles the uncertainty in the derived E_0 and excluding rates below 10^5 s^{-1} increases the uncertainty beyond reasonable limits. However, the effect of increasing the experimental range at higher energies is marginal. Excluding all rates above 10^4 s^{-1} only doubles the uncertainty. The VTST analysis of Lifshitz et al.[29] of the bromobenzene ion dissociation illustrates this point. The modeled rate curve, fit to experimental PIE data ranging from 10^3 s^{-1} to 10^5 s^{-1}, is wholly inaccurate at higher rates, but the extrapolated E_0 is nearly as accurate and precise as the results presented here.

Conclusions

Rate constants for energy selected dissociation of the halobenzene ions have been measured by TPEPICO over 4 orders of magnitude from 4×10^2 to 9×10^6 s^{-1}. Rate curves calculated by RAC-RRKM, PST, SSACM, and VTST were fitted to the experimental rate data and used to extrapolate the rates down to the threshold energy, E_0. The derived dissociation onsets were compared to the known E_0s as determined from literature thermochemical values. While RAC-RRKM provided good fits to the experimental rate curves, the predicted E_0s were significantly lower than the literature values for the chloro- and bromobenzene ion dissociations. PST provided neither good fits to the experimental rate curves for chloro- and bromobenzene, nor the correct E_0s. Although both models correctly predict the E_0 of the iodobenzene ion dissociation, PST and RAC-RRKM should not be used for barrierless ionic dissociations. Both simplified 2-parameter versions of VTST and SSACM properly fit the experimental rate curves and extrapolate to the correct E_0 for all three halobenzene ion dissociations. However, SSACM is significantly simpler to employ.

Finally, the range and quality of the experimental rate points are critical to any method of extrapolating the rate curve down to threshold. The uncertainty in the derived E_0 scales approximately linearly with the uncertainty in the experimental data points, while extending the experimental range to the lowest rates possible is vital for an accurate determination.

Acknowledgment. We thank the U.S. Department of Energy as well as the National Science Foundation (international office) for grants that support this work. B.Sz. gratefully acknowledges an OTKA international mobility grant (NN71644).

Supporting Information Available: Text giving the molecular parameters used in modeling. This material is available free of charge via the Internet at http://pubs.acs.org.

References and Notes

(1) Asamoto, B.; Dunbar, R. C. *J. Phys. Chem.* **1987**, *91*, 2804–2807.
(2) Dunbar, R. C.; Chen, J. H.; So, H. Y.; Asamoto, B. *J. Chem. Phys.* **1987**, *86*, 2081–2086.
(3) Chupka, W. A. *J. Chem. Phys.* **1959**, *30*, 191–211.
(4) Lifshitz, C. *Mass Spectrom. Rev.* **1982**, *1*, 309–348.
(5) Baer, T.; Hase, W. L. *Unimolecular Reaction Dynamics: Theory and Experiments*; Oxford University Press: New York, 1996.
(6) Light, J. C. *J. Chem. Phys.* **1964**, *40*, 3221–3229.
(7) Pechukas, P.; Light, J. C. *J. Chem. Phys.* **1965**, *42*, 3281–3291.
(8) Nikitin, E. E. *Theoret. Exp. Chem.*, **1965**, *1*, 83–90 (english transl.).
(9) Klots, C. E. *J. Phys. Chem.* **1971**, *75*, 1526–1532.
(10) Chesnavich, W. J.; Bowers, M. T. *J. Chem. Phys.* **1977**, *66*, 2306–2315.
(11) Chesnavich, W. J. *J. Chem. Phys.* **1986**, *84*, 2615–2619.
(12) Hase, W. L. *J. Chem. Phys.* **1976**, *64*, 2442–2449.
(13) Klippenstein, S. J.; Marcus, R. A. *J. Chem. Phys.* **1989**, *91*, 2280–2292.
(14) Chesnavich, W. J.; Bass, L.; Su, T.; Bowers, M. T. *J. Chem. Phys.* **1981**, *74*, 2228–2246.
(15) Hu, X.; Hase, W. L. *J. Phys. Chem.* **1989**, *93*, 6029–6038.
(16) Troe, J.; Ushakov, V. G.; Viggiano, A. A. *J. Phys. Chem. A* **2006**, *110*, 1491–1499.
(17) Klippenstein, S. J.; East, A. L. L.; Allen, W. D. *J. Chem. Phys.* **1996**, *105*, 118–140.

(18) Klippenstein, S. J.; Faulk, J. D.; Dunbar, R. C. *J. Chem. Phys.* **1993**, *98*, 243–256.
(19) Klippenstein, S. J. *Int. J. Mass Spectrom.* **1997**, *167*, 235–257.
(20) Baer, T.; Dutuit, O.; Mestdagh, H.; Rolando, C. *J. Phys. Chem.* **1988**, *92*, 5674–5679.
(21) Muntean, F.; Armentrout, P. B. *J. Phys. Chem. A* **2003**, *107*, 7413–7422.
(22) Baer, T.; Tsai, B. P.; Smith, D.; Murray, P. T. *J. Chem. Phys.* **1976**, *64*, 2460–2465.
(23) Rosenstock, H. M.; Stockbauer, R.; Parr, A. C. *J. Chem. Phys.* **1979**, *71*, 3708–3714.
(24) Rosenstock, H. M.; Stockbauer, R.; Parr, A. C. *J. Chem. Phys.* **1980**, *73*, 773–777.
(25) Dannacher, J.; Rosenstock, H. M.; Buff, R.; Parr, A. C.; Stockbauer, R.; Bombach, R.; Stadelmann, J. P. *Chem. Phys.* **1983**, *75*, 23–35.
(26) Pratt, S. T.; Chupka, W. A. *Chem. Phys.* **1981**, *62*, 153–163.
(27) Durant, J. L.; Rider, D. M.; Anderson, S. L.; Proch, F. D.; Zare, R. N. *J. Chem. Phys.* **1984**, *80*, 1817–1825.
(28) Stanley, R. J.; Cook, M.; Castleman, A. W. *J. Phys. Chem.* **1990**, *94*, 3668–3674.
(29) Lifshitz, C.; Louage, F.; Aviyente, V.; Song, K. *J. Phys. Chem.* **1991**, *95*, 9298–9302.
(30) Gefen, S.; Lifshitz, C *Int. J. Mass Spectrom. Ion. Proc.* **1984**, *58*, 251–258.
(31) Malinovich, Y.; Arakawa, R.; Haase, G.; Lifshitz, C. *J. Phys. Chem.* **1985**, *89*, 2253–2260.
(32) Yim, Y. H.; Kim, M. S. *J. Phys. Chem.* **1993**, *97*, 12122–12126.
(33) Yim, Y. H.; Kim, M. S. *J. Phys. Chem.* **1994**, *98*, 5201–5206.
(34) Lim, S. H.; Choe, J. C.; Kim, M. S. *J. Phys. Chem. A* **1998**, *102*, 7375–7381.
(35) Baer, T.; Kury, R. *Chem. Phys. Lett.* **1982**, *92*, 659–662.
(36) Fogleman, E. A.; Koizumi, H.; Kercher, J. P.; Sztáray, B.; Baer, T. *J. Phys. Chem. A* **2004**, *108*, 5288–5294.
(37) Baer, T.; Li, Y *Int. J. Mass Spectrom.* **2002**, *219*, 381–389.
(38) Kercher, J. P.; Stevens, W. R.; Gengeliczki, Z.; Baer, T *Int. J. Mass Spectrom.* **2007**, *267*, 159–166.
(39) *Gaussian 03, Revision C.02* Frisch, M. J.; Trucks, G. W.; Schlegel, H. B.; Scuseria, G. E.; Robb, M. A.; Cheeseman, J. R.; Montgomery, J. A.; Vreven, T.; Kudin, K. N. ; Burant, J. C.; Millam, J. M.; Iyengar, S. S.; Tomasi, J.; Barone, V.; Mennucci, B.; Cossi, M.; Scalmani, G.; Rega, N.; Petersson, G. A.; Nakatsuji, H.; Hada, M.; Ehara, M.; Toyota, K.; Fukuda, R.; Hasegawa, J.; Ishida, M.; Nakajima, T.; Honda, Y.; Kitao, O.; Nakai, H.; Klene, M.; Li, X.; Knox, J. E.; Hratchian, H. P.; Cross, J. B.; Adamo, C.; Jaramillo, J.; Gomperts, R.; Stratmann, F.; Yazyev, O.; Austin, A. J.; Cammi, R.; Pomelli, C.; Ochterski, J. W.; Ayala, P. Y.; Morokuma, K.; Voth, G. A.; Salvador, P.; Dannenberg, J. J.; Zakrzewski, V. G.; Dapprich, S.; Daniels, A. D.; Strain, M. C.; Farkas, Ö.; Malick, D. K.; Rabuck, A. D.; Raghavachari, K.; Foresman, J. B.; Ortiz, J. V.; Cui, Q.; Baboul, A. G.; Clifford, S.; Cioslowski, J.; Stefanov, B. B.; Liu, G.; Liashenko, A.; Piskorz, P.; Komáromi, I.; Martin, R. L.; Fox, D. J.; Keith, T.; Al-Laham, M. A.; Peng, C. Y.; Nanayakkara, A.; Challacombe, M.; Gill, P. M. W.; Johnson, B.; Chen, W.; Wong, M. W.; Gonzalez, C.; Pople, J. A. Gaussian, Inc.: Wallingford, CT, 2004
(40) Feller, D. *J. Comput. Chem.* **1996**, *17*, 1571–1586.
(41) Schuchardt, K. L. *J. Chem. Inf. Model.* **2007**, *47*, 1045–1052.
(42) Pedley, J. B. *Thermochemical Data and Structures of Organic Compounds*; Thermodynamics Research Center: College Station, TX, 1994.
(43) Kwon, C. H.; Kim, H. L.; Kim, M. S. *J. Chem. Phys.* **2002**, *116*, 10361–10371.
(44) Chase, M. W. *NIST-JANAF Thermochemical Tables*; 4th ed.; American Institute of Physics: New York, 1998.
(45) Lau, K.-C.; Ng, C. Y *J. Chem. Phys.* **2006**, *124*, 044323/1-044323/9.
(46) Blanksby, S. J.; Ellison, G. B. *Acc. Chem. Res.* **2003**, *36*, 255–263.
(47) Butcher, V.; Costa, M. L.; Dyke, J. M.; Ellis, A. R.; Morris, A. *Chem. Phys.* **1987**, *115*, 261–267.
(48) Dunbar, R. C. *Mass Spectrom. Rev.* **1992**, *11*, 309–339.
(49) Troe, J. *J. Chem. Phys.* **1983**, *79*, 6017–6029.
(50) Brouwer, L.; Cobos, C. J.; Troe, J.; Dubal, H. R.; Crim, F. F. *J. Chem. Phys.* **1987**, *86*, 6171–6182.
(51) Troe, J. *J. Chem. Soc., Faraday Trans.* **1997**, *93*, 885–891.
(52) Troe, J. *J. Chem. Phys.* **1996**, *105*, 6249–6262.

JP807930K